Supporting Information

Electrochemically-Formed Disordered Rock Salt ω-$Li_xV_9Mo_6O_{40}$ as a Fast-Charging Li-Ion Electrode Material

Daniel D. Robertson,[a] Charlene Z. Salamat,[a] David J. Pe,[a] Helen Cumberbatch,[a] David Agyeman-Budu,[b] Johanna Nelson Weker,[b] Sarah H. Tolbert[a,c,d,*]

[a]Department of Chemistry and Biochemistry, UCLA, Los Angeles, California 90095, United States

[b]Stanford Synchrotron Radiation Lightsource, SLAC National Accelerator Laboratory, Menlo Park, California 94025, United States

[c]Department of Materials Science and Engineering, UCLA, Los Angeles, California 90095, United States

[d]The California NanoSystems Institute, UCLA, Los Angeles, California 90095, United States

*Corresponding Author. Email: tolbert@chem.ucla.edu.

Charge Neutrality within the $V_9Mo_6O_{40}$ Phase

While VMO is synthesized in air or oxygen, indicating that the material is stable to further oxidation to at least 650ºC, the established chemical formula of $V_9Mo_6O_{40}$ is slightly off of charge balance if all metal ions are fully oxidized (V^{5+} and Mo^{6+}), and all oxygens are O^{2-}. One possible explanation for this is partial reduction of the transition metals: in the unit cell with fifteen metal ions, one metal ion must be reduced by one oxidation state (V^{4+} or Mo^{5+}). Alternatively, all metal ions could remain in their highest oxidation state, with the charge balanced by one oxygen vacancy for every two unit cells. Ultimately, the very small amount of either reduced metal ions or oxygen vacancies makes it difficult to conclusively validate either hypothesis. While our XPS does not show evidence of reduced transition metal species in pristine VMO, the initial crystallographic studies on the compound also did not identify any oxygen vacancies.

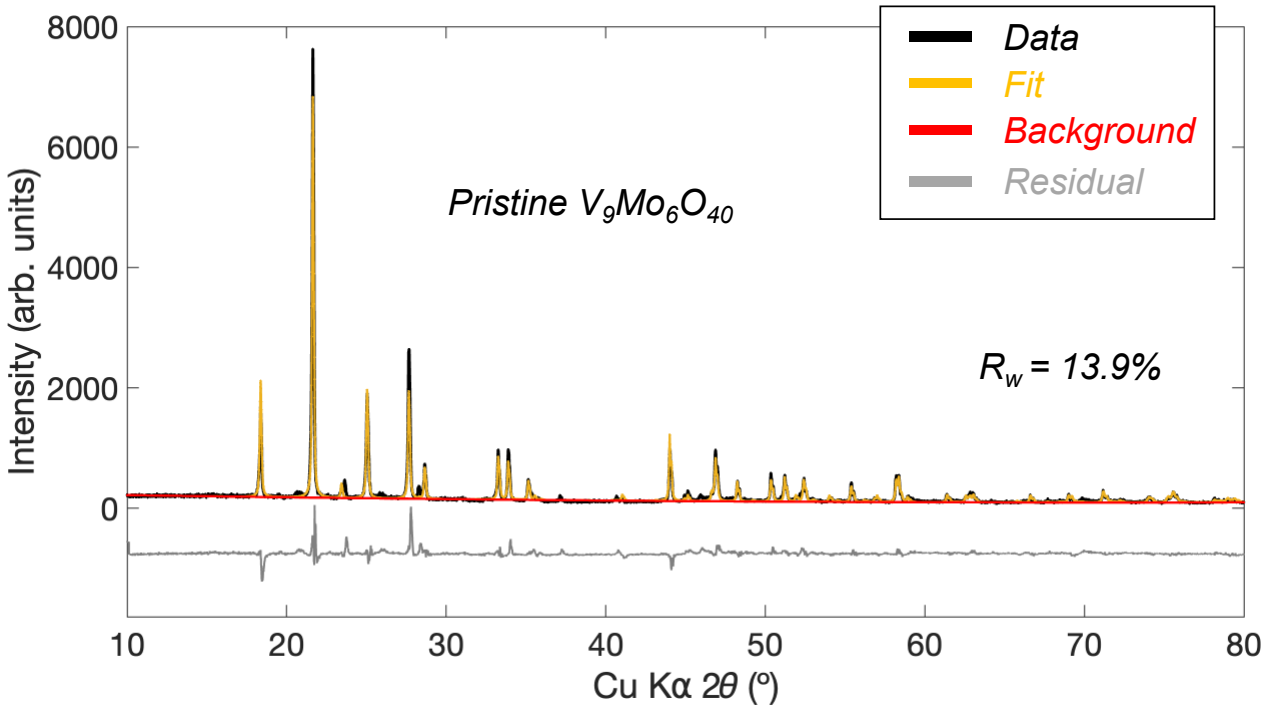

Figure S1. Rietveld refinement of laboratory powder X-ray diffraction data on pristine VMO. The refinement confirms a close match with previously reported lattice parameters with a strongly oriented powder texture due to the platelike morphology of the VMO material.

Table S1. Results of the Rietveld refinement shown in Figure S1.

Parameter	Value
Phase Fraction	1
Space Group	C2
Lattice constant	a = 19.4 Å
	b = 3.63 Å
	c = 4.12 Å
	β = 90.4°
Texture Index (Spherical Harmonic)	1.96
R_w	13.9

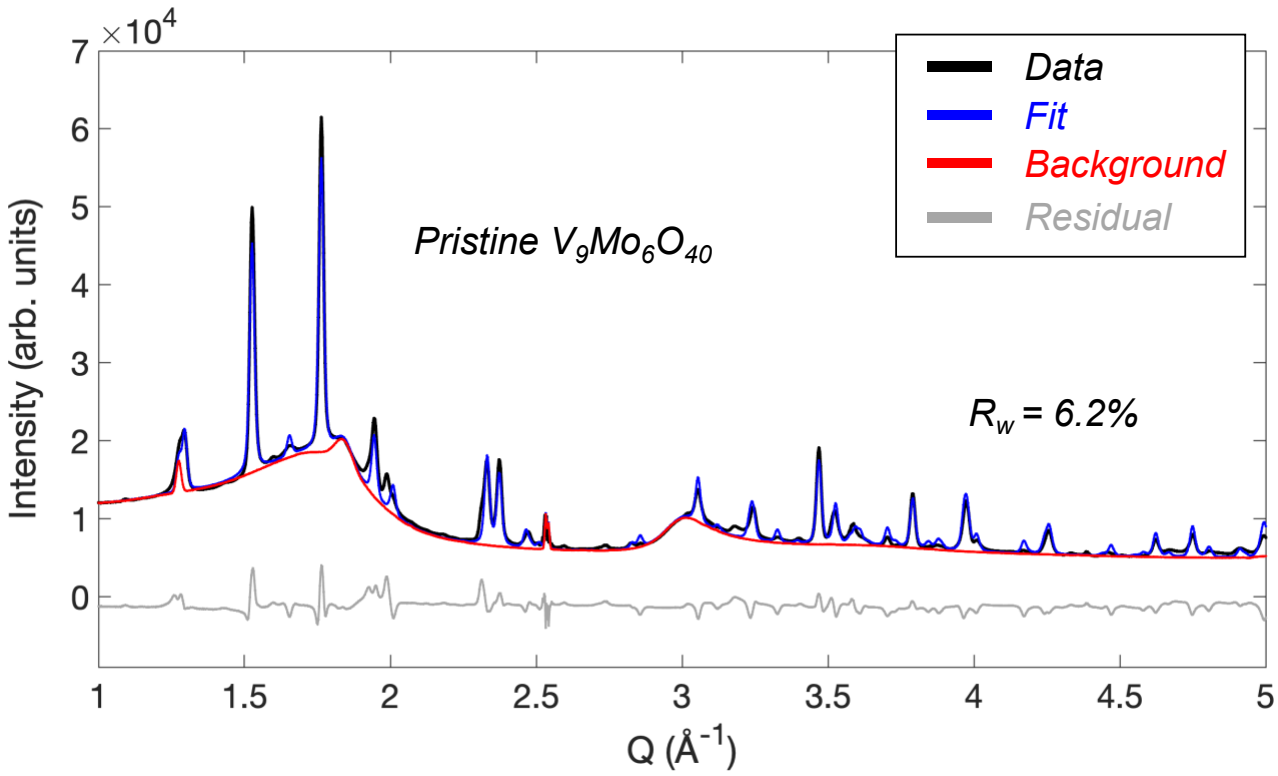

Figure S2. Rietveld refinement of synchrotron powder X-ray diffraction data on pristine VMO pellet electrodes in an AMPIX cell. This refinement confirms a close match with the previously reported lattice parameters, but there is less texture due to the pellet electrode format. The background is from the cell components and electrolyte.

Table S2. Results of the Rietveld refinement shown in Figure S2.

Parameter	Value
Phase Fraction	1
Space Group	C2
Lattice constant	a = 19.4 Å
	b = 3.62 Å
	c = 4.11 Å
	β = 90.4°
Texture Index (Spherical Harmonic)	1.04
R_w	6.1

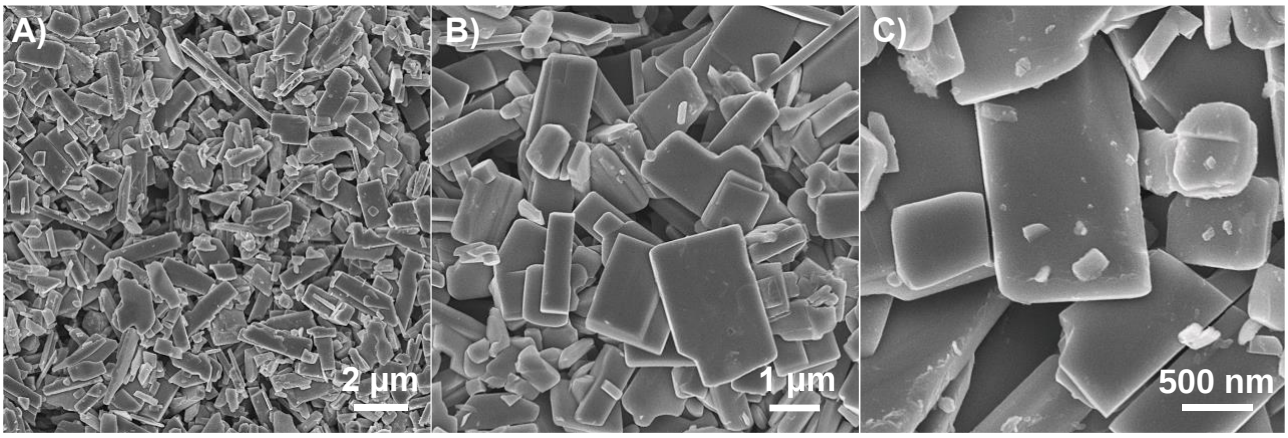

Figure S3. Additional scanning electron microscopy characterization of pristine bulk VMO.

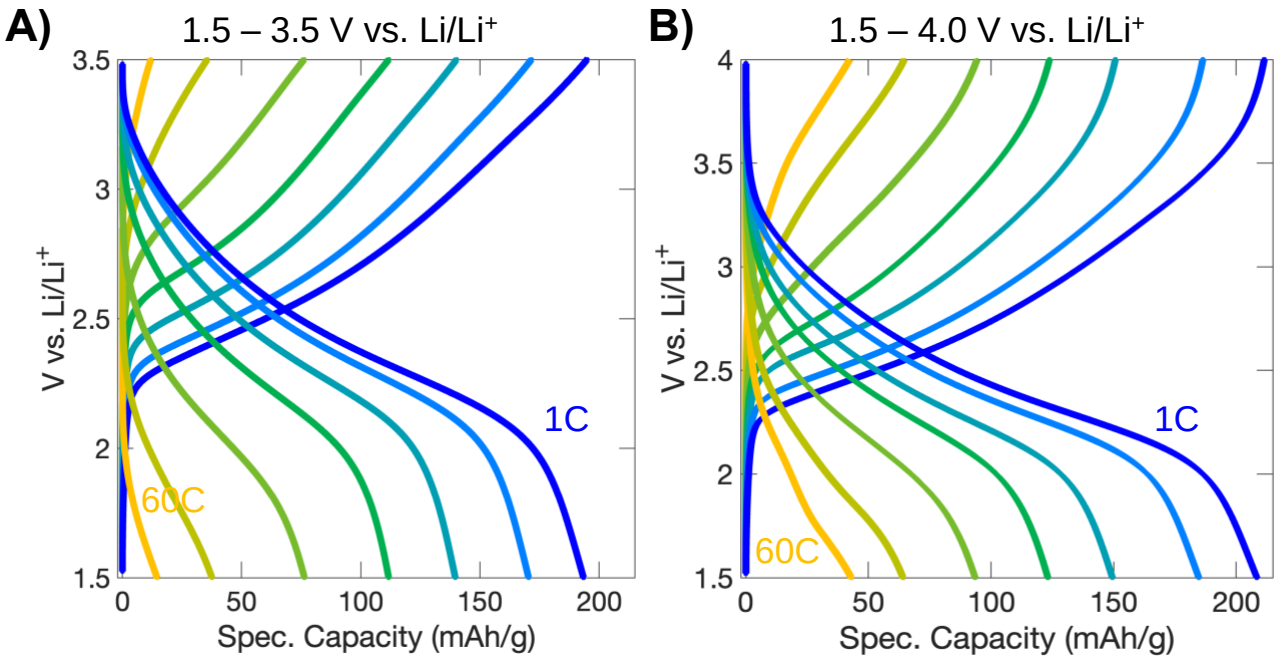

Figure S4. Rate-dependent galvanostatic profiles from cycling data for bulk VMO in Figure 2B of the main text with **A)** 3.5 V upper cutoff voltage and **B)** 4.0 V upper cutoff voltage.

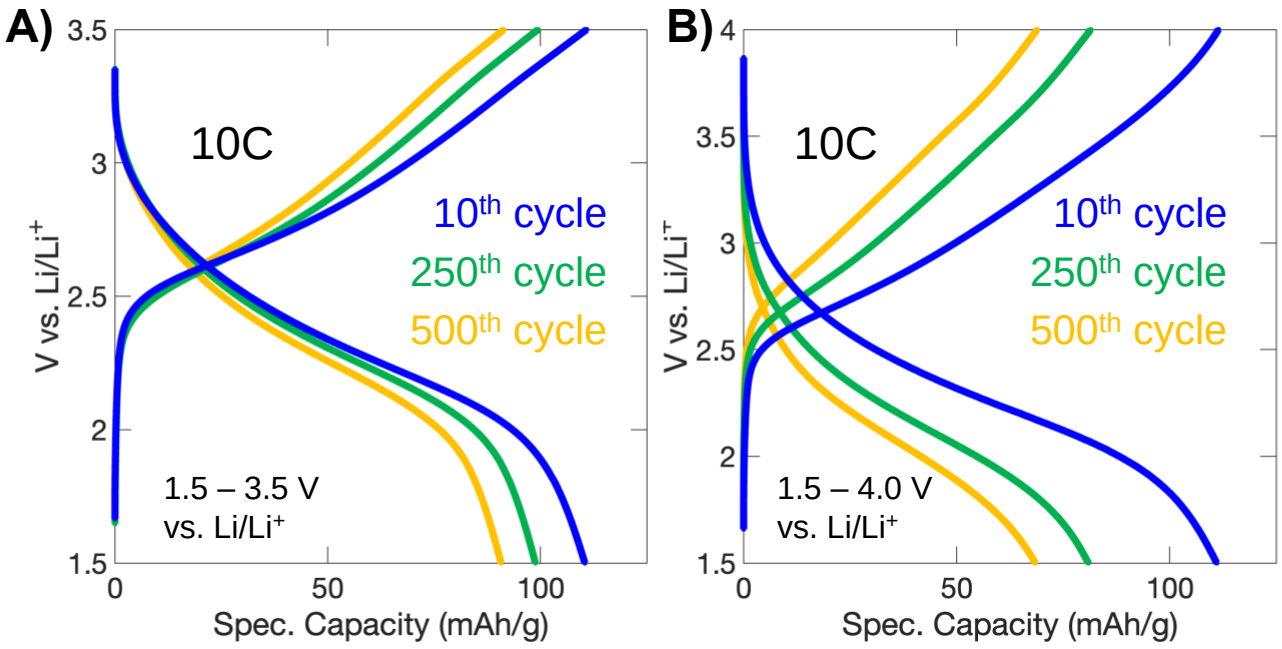

Figure S5. Galvanostatic profiles from long term cycling data in Figure 2C of the main text with **A)** 4.0 V upper cutoff voltage and **B)** 3.5 V upper cutoff voltage. The capacity occurs gradually and shows no major changes in the shape of the profile.

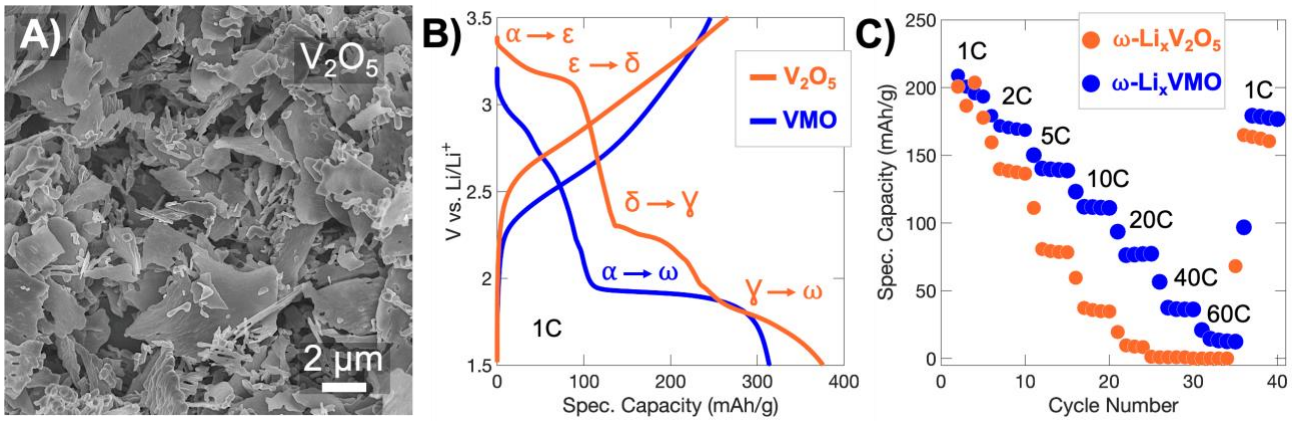

Figure S6. Comparison between V_2O_5 and VMO. A) Scanning electron micrograph of α-V_2O_5 produced by the same freeze-drying-based synthetic route that was used for VMO in this work. B) Galvanostatic profile of the first cycle and C) galvanostatic rate performance for ω-phase V_2O_5 and VMO electrodes cycled between 1.5 - 3.5 V vs. Li/Li^+. In panel B, V_2O_5 shows a multistep pathway involving multiple first-order phase transitions before transforming to a rock salt phase, while VMO transforms directly to the rock salt phase, likely due to increased rigidity in its crystal structure. In panel C, VMO shows improved rate capability in the voltage window, potentially from the distorted microstructure shown in the main text.

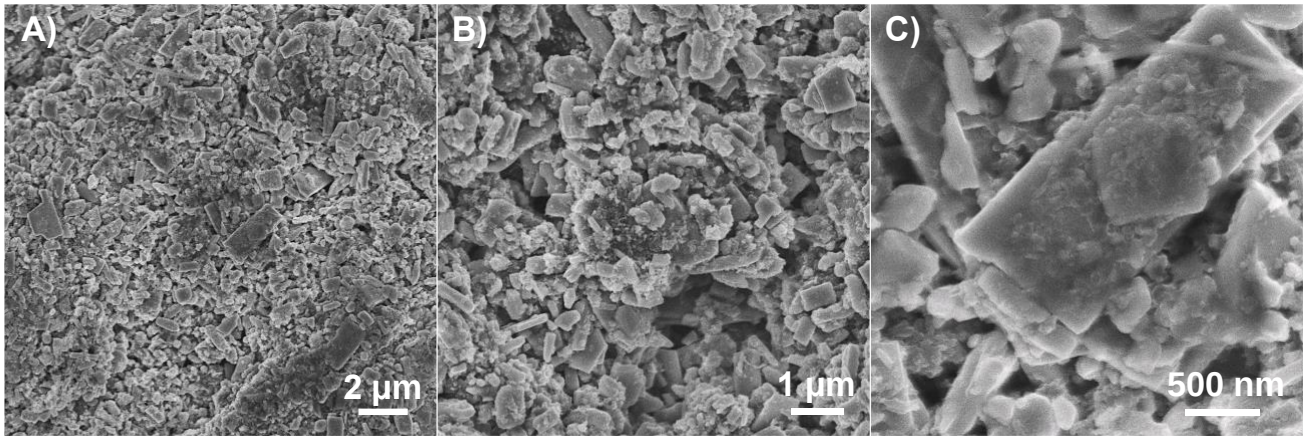

Figure S7. Additional scanning electron microscopy characterization of a cycled VMO electrode, showing retention of morphology after transformation to the disordered rock salt phase.

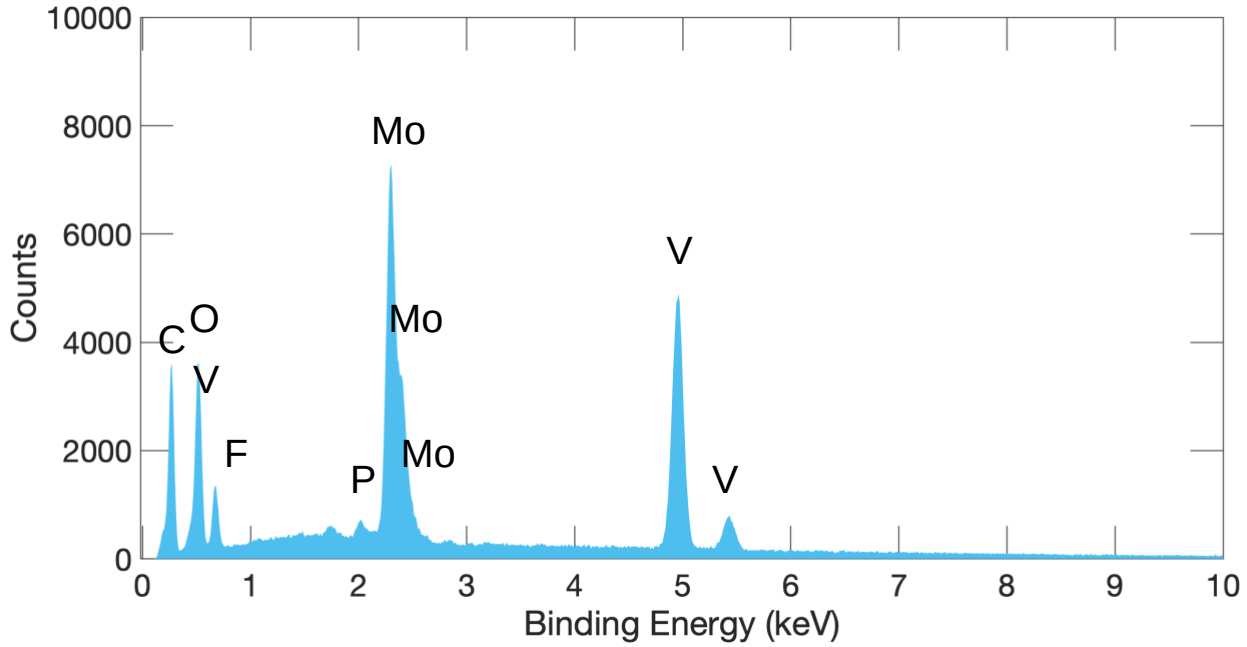

Figure S8. Energy dispersive spectroscopy (EDS) elemental characterization of a cycled VMO electrode, confirming the presence of both V and Mo in the disordered rock salt electrode.

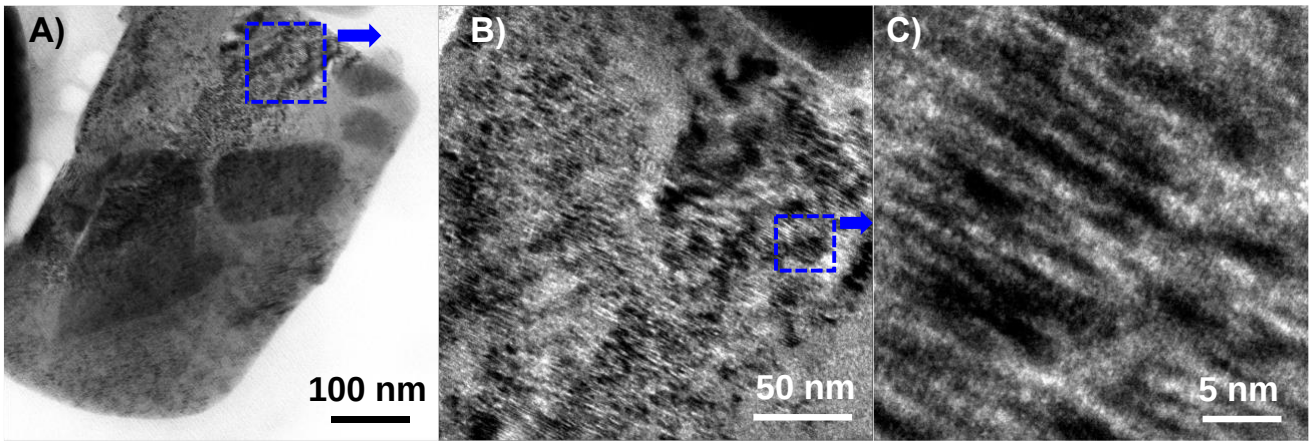

Figure S9. Additional high resolution transmission electron microscopy of the disordered rock salt VMO showing the distorted lamellar morphology that forms after the first cycle.

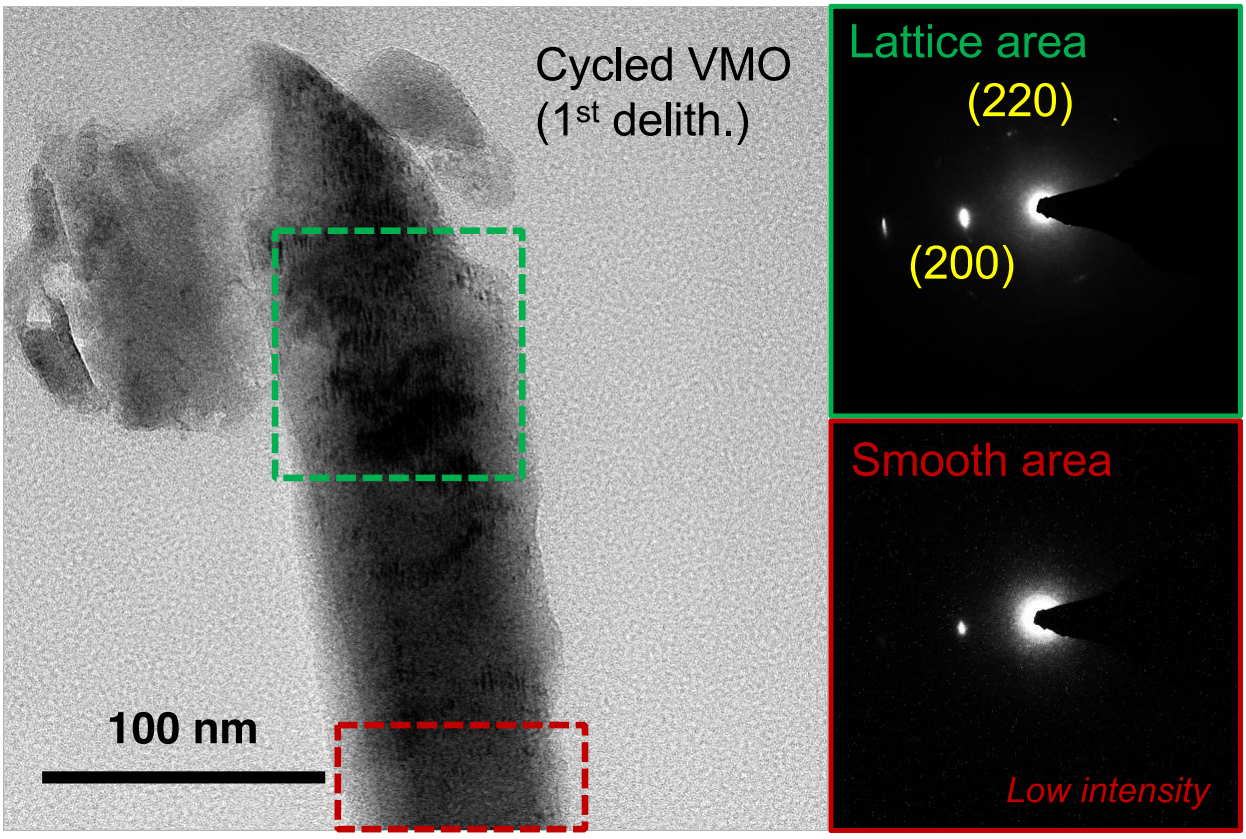

Figure S10. Electron diffraction of cycled VMO shows that the distorted, lamellar morphology corresponds to the rock salt structure.

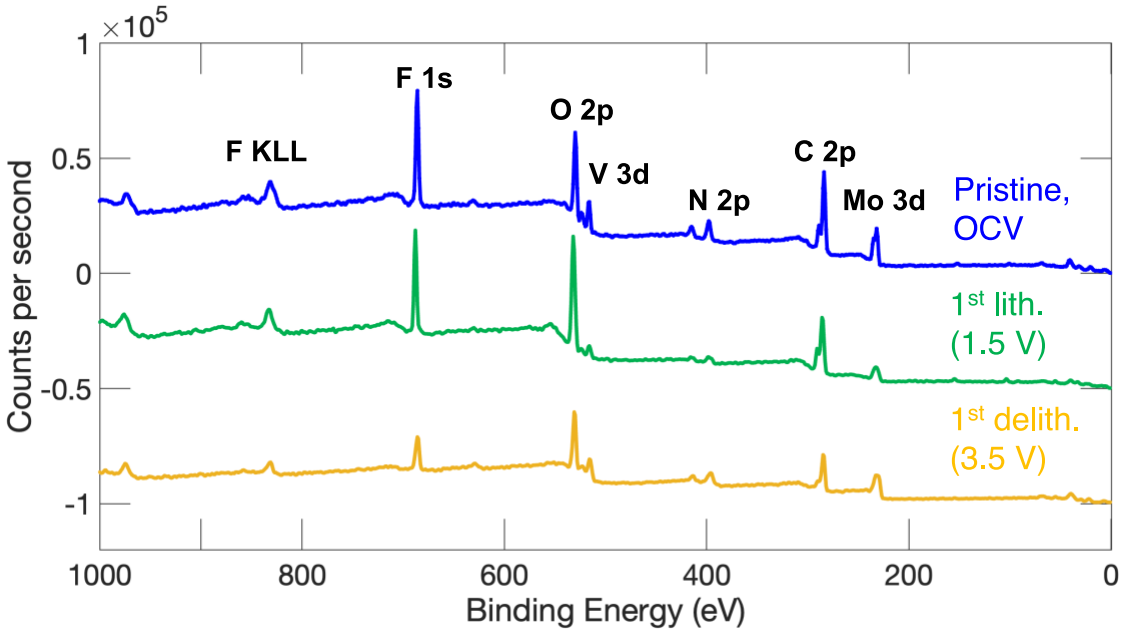

Figure S11. Full XPS survey scans from the high-resolution XPS data shown in Figure 6 of the main text.

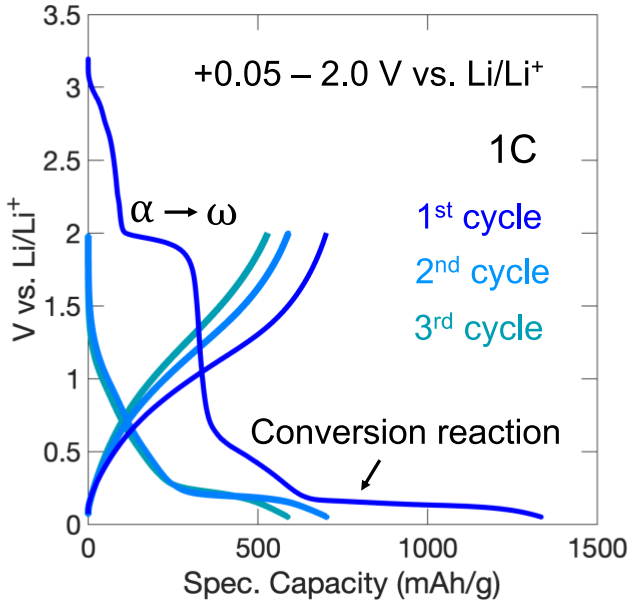

Figure S12. Low voltage cycling behavior of VMO electrode. V_2O_5, which also forms a disordered rock salt phase during electrochemical cycling, has been reported to undergo additional lithiation with high rate capability at low voltage. While VMO does have further lithiation at low voltage, it appears to be accompanied by the conversion reaction, where oxide is reduced to metal.